Concurrent evolution of vortex phase diagram and charge density wave order in kagome superconductor $CsV_3Sb_{5-x}Sn_x$

Hongyu Li(李弘禹)[1], Huachen Rao(饶华琛)[1], Xingchen Zhou(周星辰)[1], Houpu Li(李厚朴)[2], Zhao Gong(巩钊)[1], Tao Wu(吴涛)[1,3], Ziji Xiang(项子雾)[1,3], and Xianhui Chen(陈仙辉)[1,2,3*]

[1]Hefei National Research Center for Physical Sciences at the Microscale, University of Science and Technology of China, Hefei, 230026, China

[2]Department of Physics, University of Science and Technology of China, Hefei, 230026, China

[3]Hefei National Laboratory, Hefei, 230088, China

2026 年 9 月 30 日

Abstract

The kagome lattice superconductor CsV_3Sb_5 display a surprisingly rich vortex phase diagram, which adds to the unique properties of its superconducting state that develops from a charge density wave (CDW) state. The coexisting superconductivity and CDW in CsV_3Sb_5 can be effectively manipulated via chemical doping. Here we systematically investigate the vortex matter phases of $CsV_3Sb_{5-x}Sn_x$ with different doping concentrations x under in-plane magnetic fields via electrical transport, magnetic torque and ac susceptibility measurements. Three superconducting regions are identified in the phase diagrams of $CsV_3Sb_{5-x}Sn_x$, corresponding to superconductivity developing from the 2×2 CDW state ($x = 0, 0.06$), short-ranged charge stripe state ($x = 0.09$) and fluctuating CDW state ($x = 0.25$); each is characterized by distinct behavior of vortex dynamics. The results reveal that the CDW behavior in the normal state exerts a remarkable influence on the superconducting state, which indicates unusual interplay between CDW and superconductivity in $CsV_3Sb_{5-x}Sn_x$.

Keywords: charge density wave, vortex dynamics, kagome superconductor

1. Introduction

Investigations on vortex behaviors can reveal characteristic superconducting properties [1]. In strongly anisotropic layered superconductors, enhanced thermal fluctuations can create a broad phase regime of vortex liquid (VL, which crosses over to the normal state), or even more peculiar vortex matters in the field-temperature (H-T) phase diagram [2,3]. In charge-ordered or spin-ordered cuprate superconductors,

*Corresponding author. E-mail:chenxh@ustc.edu.cn

exotic vortex states had been identified such as anomalous vortex liquid state [4,5] and viscous vortex liquid state [6]. The kagome lattice compound CsV_3Sb_5, in which superconductivity develops from a normal state with triple-Q CDW order [7], has been identified as anisotropic multigap superconductivity [8–10]; recent work reveals a exquisite vortex phase diagram with weak bulk pinning [11].

The CDW states in CsV_3Sb_5 can be deliberately tuned through chemical substitution. With the substitution of Ta, Nb or Ti on the vanadium site, CDW can be gradually suppressed and a more isotropic superconducting order parameter emerges in the undistorted kagome phase [12,13]; a very weak bulk vortex pinning is also identified [14,15]. Upon Sn doping, a short-ranged single-Q charge-stripe phase emerges at critical doping level $x = 0.07$ and gradually fluctuates at higher doping level [16–19]. The superconducting critical temperature T_c is suppressed within the doping range where the stripelike CDW can be unambiguously captured by both charge transport and spectroscopic measurements [18,19], demonstrating that modifications to the CDW configuration exert a tangible influence on the superconducting state.

Three distinct superconducting regimes emerge on the phase diagram of $CsV_3Sb_{5-x}Sn_x$ [Fig. 1(d)], corresponding to superconductivity developing from triple-Q CDW state ($x \leqslant 0.06$; SC-I), short-ranged charge-stripe state ($0.07 \leqslant x < 0.12$; SC-II) and fluctuating CDW state ($x \geqslant 0.12$, harboring very short-ranged single-Q charge correlation; SC-III), respectively [19]. In this work, combining electrical transport, magnetic torque, and ac susceptibility measurements, we systematically map out the $H-T$ phase diagrams of four distinct doping compositions of Sn-doped CsV_3Sb_5 ($x = 0$, 0.06, 0.09 and 0.25) under in-plane magnetic fields. In SC-I, there is an order–disorder transition in vortex solid (VS) state. In SC-II, a wide phase regime with both nonzero electrical resistance and diamagnetic loop is identified as heterogeneous vortex glass state, arising from the distribution of local T_c. In SC-III, a pronounced peak effect is clearly resolved, manifesting reinforced flux pinning upon the occurrence of order–disorder transformation in VS state. Our results demonstrate that the CDW order persisting in the normal state substantially affects the superconducting behaviors in $CsV_3Sb_{5-x}Sn_x$.

2. Results

2.1. Electrical transport and torque magnetometry measurements

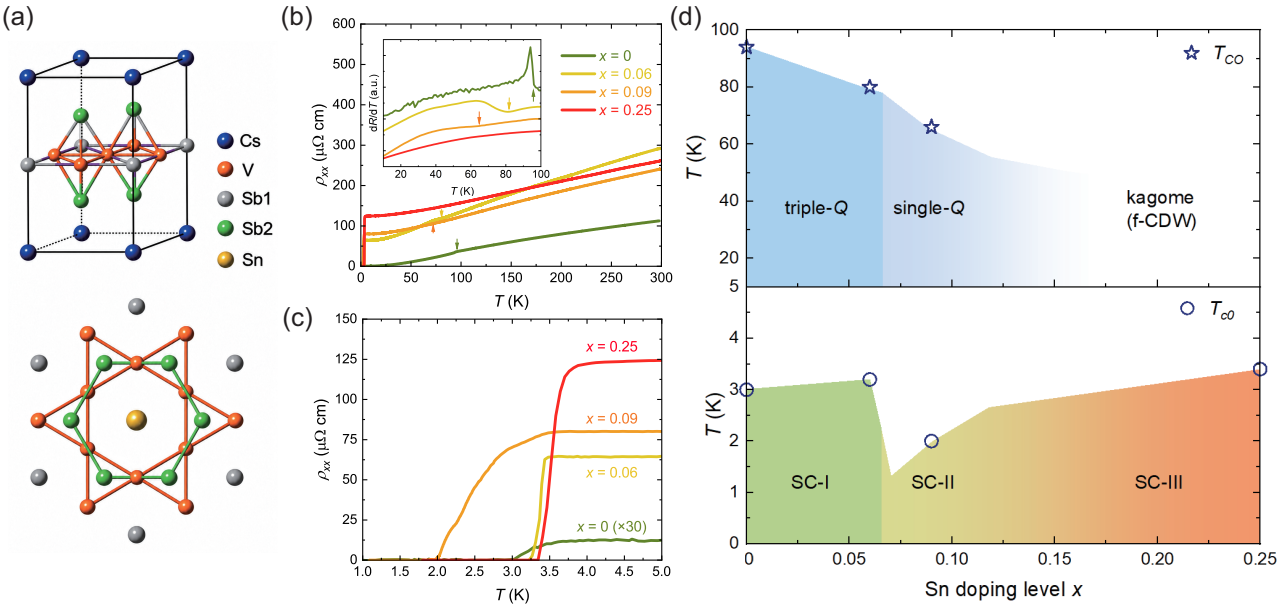


Fig. 1. (a) Crystal structure of CsV_3Sb_5 and a schematic showing the position of substituted Sn atoms. (b) ρ_{xx} measured from 1.8 K to 300 K in five samples of $CsV_3Sb_{5-x}Sn_x$ with different x. Inset displayed temperature derivative of longitudinal resistivity, $d\rho_{xx}/dT$, as a function of T. Arrows indicate the onset of anomaly manifesting the CDW transition. At x = 0.30, this transition becomes invisible. (c) A zoomed view of low-T ρ_{xx} showing the superconducting transitions. (d) Doping phase diagram of $CsV_3Sb_{5-x}Sn_x$ showing the evolution of the CDW (b) and superconductivity (c) upon increase of Sn doping level x. This phase diagram is constructed based on the data reported in Ref. [19]. Four distinct doping concentrations were characterized via measurements in this paper, and the results are displayed as stars and circles in panel (d).

Single crystals of $CsV_3Sb_{5-x}Sn_x$ with doping concentrations of x = 0, 0.06, 0.09, and 0.25 were synthesized using the flux growth technique (see Supplemental Materials [20]). Previous results indicate the Sn dopant (substitutions to the Sb atoms) favour to substitute the Sb atoms in the V_3Sb kagome plane, as shown in [Fig. 1(a)] [16]. Using electrical resistivity measurement [Fig. 1(b) and (c)], we established the phase diagram for $CsV_3Sb_{5-x}Sn_x$ [Fig. 1(d)]. For the samples with $x = 0$ and 0.06, the resistivity curves exhibit a distinct sharp transition, which serves as a characteristic signature of the CDW phase transition. In contrast, only a subtle inflection crossover is observed in the resistivity curves for $x = 0.09$, identified as a short-ranged charge stripe order by previous studies [18]. At higher doping level $x = 0.25$, no evident anomaly can be identified in the resistivity profiles, which implies a fluctuating-type charge order at this composition. The emergence of a two-dome superconducting phase is in good agreement with previous experimental studies [16–19].

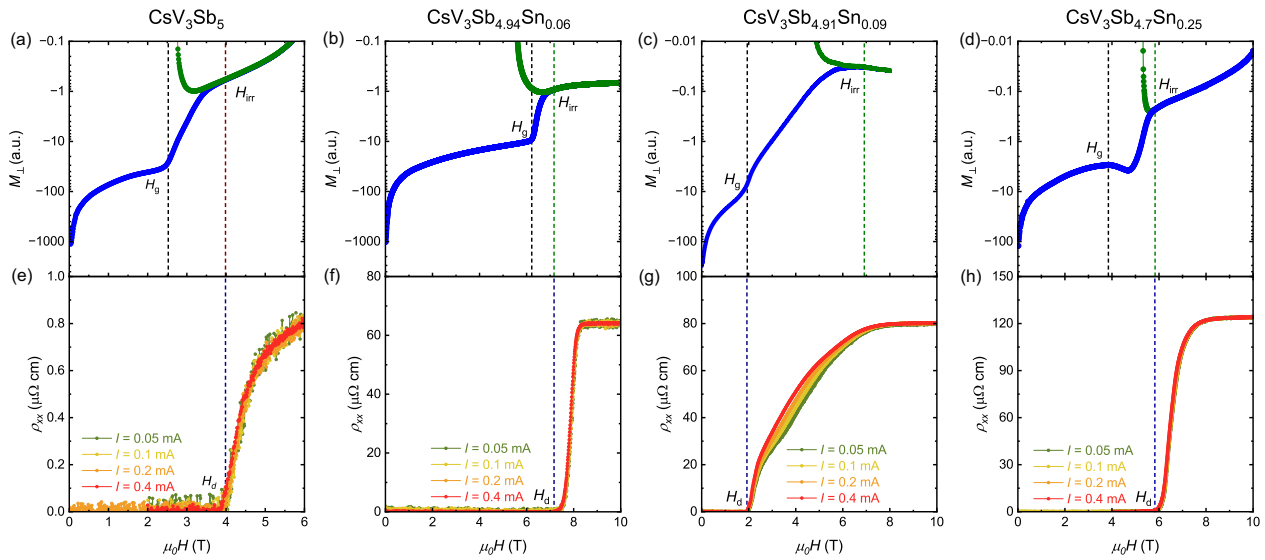


Fig. 2. Magnetic torque [$M_\perp = \tau/\mu_0 H$, (a)-(d)] and magnetoresistance [(e)-(h)] versus fields at $T = 0.4$ K for $CsV_3Sb_{5-x}Sn_x$ ($x = 0$, 0.06, 0.09 and 0.25). In the torque curves the blue curve denotes the fields sweep from zero upward and the green curve the fields sweep from high field downward. H^* is the critical field in (a)-(c) where the magnetization decays rapidly. We define H_g as the kink on the blue curve in (d), which we interpret as the transition from vortex lattice to vortex glass. The field at which the up- and down-sweep torque traces cease to overlap is taken as the irreversibility field H_{irr}. The characteristic field H_d is extracted from magnetoresistance curves where zero resistance behavior disappears.

Fig. 2 shows the magnetic torque and magnetoresistance traces at $T = 0.4$ K for $x = 0$, 0.06, 0.09 and 0.25. The magnetoresistance and magnetic torque data of different temperatures are summarized in Supplemental Materials [20]. In panels (a)–(d) the blue curves are the magnetization perpendicular to the applied fields measured while sweeping the fields up from zero. For $x = 0$ and 0.06 samples, a clear kink appears at H^* where the superconducting critical current density J_c decays rapidly [Fig. 2(a), (b)], known as the vortex avalanche effect (see more details in Supplemental Materials [20]) [21]. Incoming vortices fail to relax into an equilibrium state in vortex lattice, leading to avalanche behavior, which is commonly regarded as a definitive signature of vortex solid (VS).

Scanning tunneling microscopy (STM) measurements reveal nearly perfect Abrikosov vortex lattice in pristine CsV_3Sb_5 single crystals [22]. The formation of vortex lattice indicates that vortices in CsV_3Sb_5 are barely pinned by randomly dispersed impurities, which enables the emergence of vortex lattice softening induced peak effect (see more explanations in Supplemental Materials [20]); this had indeed been experimentally detected in previous reports when magnetic fields is aligned c-axis [11,15]. However, no analogous peak response is detected for in-plane magnetic fields [Fig. 2(a)]. Such distinct vortex pinning behaviors for fields parallel to the ab plane and to the c axis have been widely investigated in anisotropic superconductors such as MgB_2 [23] and $YBa_2Cu_3O_7$ [24]. In MgB_2, the peak effect also disappears in the susceptibility measurements when the magnetic field is turned away from c axis since the pinning of vortices is much more efficient for $H \parallel ab$ [23]. In $YBa_2Cu_3O_7$, the peak effect due to the enhanced vortex pinning by the twin boundaries disappears once the applied fields tilts by 4° away from the c direction [24].

In standard phenomenology of conventional type-II superconductors, the irreversibility field $H_{\rm irr}$ where magnetization hysteresis closes coincides with the depinning field $H_{\rm d}$ defined as the threshold field for the vanishing of zero resistance [Fig. 2(a)-(b), (d)-(f) and (h)]; both roughly coincide with the solid-liquid transition of the vortex matter [2]. In addition, nearly overlapping magnetoresistance curves measured under varied excitation currents confirm homogeneity of the superconducting state across these three samples [Fig. 2(e), (f) and (h)]. In sharp contrast, the $x = 0.09$ sample exhibits distinct behaviors. A characteristic field H^* can be clearly resolved as a kink in blue curves of Fig. 2(c); unlike the other three compositions whose H^* and $H_{\rm g}$ lies within the zero-resistance regime, this characteristic field coincides precisely with $H_{\rm d}$ where zero resistance is destroyed, as illustrated in panels (c) and (g) of Fig. 2. Generally, zero resistance (under small electric fields) persists in VS, whereas the closure of magnetization hysteresis marks the transition into VL phase accompanied by mobile vortices and finite electrical dissipation. Remarkably, the $x = 0.09$ sample features an extensive phase region where diamagnetic hysteresis coexists with finite resistance over a broad field range, as verified in Fig. 2(c) and (g). Meanwhile, the magnetoresistance curves display pronounced non-ohmic behavior under different measuring currents. Collectively, these experimental signatures point to an inhomogeneous distribution of local energy scales throughout the sample, which is discussed in detail below.

For the sample with $x = 0.25$, the magnitude of diamagnetism does not decrease monotonically with increasing magnetic fields at the characteristic field $H_{\rm g}$. Instead, a distinct peak emerges on the blue curve in Fig. 2(c). This characteristic behavior is known as the peak effect (see Supplemental Materials [20]) [25–28]. As a typical signature of enhanced pinning strength in vortex glass state, the peak effect has been widely reported in various type-II superconductors, such as NbZr [29], YBCO [24,30], and 2H-$NbSe_2$ [31].

2.2. AC susceptibility measurements

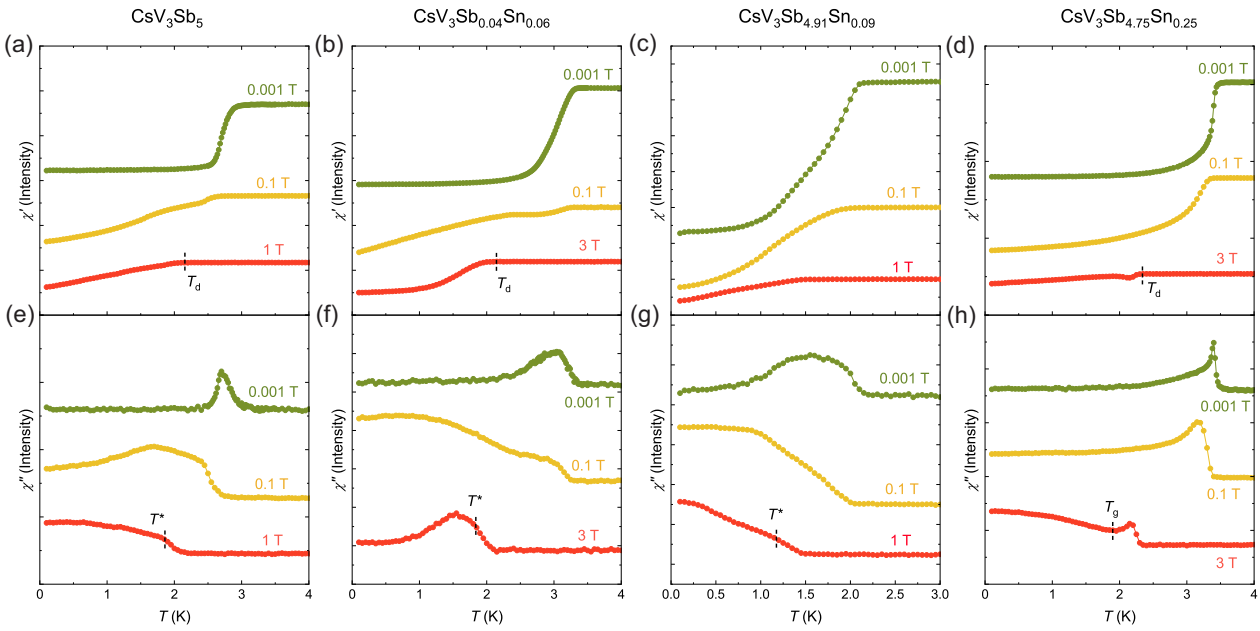


Fig. 3. Temperature-dependent real-part [(a) - (d)] and imaginary-part [(e) - (h)] curves of ac susceptibility for four compositions of $CsV_3Sb_{5-x}Sn_x$ (x = 0, 0.06, 0.09 and 0.25) measured under various applied dc magnetic fields. The measurements were performed from 0.1 K to 4 K with an alternating excitation field H_{ac} = 1 Oe at a fixed frequency of 1000 Hz. The crossover on $\chi''(T)$ curves in (e)-(g) appear at the critical temperature T^*, indicating the formation of ordered VS. We define T_g as the kink on $\chi''(T)$ curves in (h), which we interpret as the transition from vortex lattice to vortex glass. T_d is the critical temperature on $\chi''(T)$ curves where diamagnetism arises. Note that in x = 0.09 sample, diamagnetism appears at a relatively high temperature [19]; limited by the measurement precision of ac susceptibility, we are unable to precisely determine the value of T_d.

For a superconductor, the real component $\chi'(T)$ of ac susceptibility reflects its diamagnetic shielding capability and the imaginary component $\chi''(T)$ reflects energy dissipation [32,33]. Under a weak applied alternating fields (typically several Oe), $\chi'(T)$ develops a step-like diamagnetic drop at $T = T_c$, marking the onset of bulk superconductivity. Correspondingly, the imaginary component $\chi''(T)$ displays a prominent peak associated with maximum internal energy dissipation, which emerges slightly below T_c [33]. The origin of the peak observed in the imaginary part of the ac susceptibility remains controversial [34–39] (see further explanations in Supplemental Materials [20]).

Turning to our experimental data measured under dc field of 10 Oe in Fig. 3, the $\chi'(T)$ of $x = 0$, 0.06 and 0.25 samples rapidly saturates into full diamagnetism across the superconducting transition [Fig. 3(a)-(b), (d)], accompanied by well-defined sharp peaks in $\chi''(T)$ [Fig. 3(e)–(f), (h)]. Such features coincide with the canonical behavior of conventional type-II superconductors [32]. In stark contrast, the $x = 0.09$ sample exhibits an extraordinarily broad transition in $\chi'(T)$ without distinct step-like features [Fig. 3(c)] and its $\chi''(T)$ curve also evolves into a broad hump [Fig. 3(g)]. Similar broadened $\chi''(T)$ anomalies have been widely reported in granular superconductors [33,40,41] and polycrystalline high-T_c superconductors [42]. For polycrystals with uniform intrinsic T_c, broad $\chi''(T)$ signals persist below T_d, originating from intergrain Josephson weak links with broadly distributed coupling strengths and corresponding spread of Josephson critical currents [42]. For granular superconductors, scattered T_c among discrete superconducting grains yields broadened or even multiple separated peaks in $\chi''(T)$, each corresponding to the superconducting transition of individual grain subsets [41]. Intergrain Josephson weak links in granular systems further contribute to the broadening of the imaginary susceptibility spectra [33]. Given that our Sn-substituted CsV_3Sb_5 samples are single crystals, we assign the pronounced broad $\chi''(T)$ peak of the $x = 0.09$ sample [Fig. 3(c)] to intrinsic spatial inhomogeneity of local T_c across the crystal. Noticeably, $\chi''(T)$ fails to vanish down to $T = 1$ K, which may be connected to the residual quasiparticles in superconducting state [19]. The grains with different T_c may have distinct critical currents under magnetic fields, contributing the non-ohmic behaviors in magnetoresistance curves [Fig. 2(g)]. The proposed local T_c distribution in the $x = 0.09$ sample is fully compatible with the conclusions from previous studies, in which superconductivity has a spatial variation of the superconducting order parameter and there are no non-superconducting regions in real space for $x = 0.09$ sample [19].

When the applied dc fields suffice to give rise to the mixed state, distinct features emerge for the $x = 0$ and $x = 0.06$ samples. As clearly revealed from $\chi''(T)$ curves: $x = 0$ under 1 T [Fig. 3(e)] and $x = 0.06$ under 3 T [Fig. 3(f)], finite $\chi''(T)$ signals emerge below T_d, which is commonly ascribed to the formation of VS [43]. Slightly below T_d, a noticeable kink develops in $\chi''(T)$ at a characteristic temperature T^*. Below

T^*, analogous broad peaks were previously observed in $YBa_2Cu_3O_7$ and interpreted as a consequence of weakly pinned vortex lattice development [44].

For the $x = 0.09$ sample subjected to a large in plane magnetic field of 1 T [Fig. 3(g)], $\chi''(T)$ increases monotonically with decreasing temperature, and an inflection point is identified at the characteristic temperature ($T^* = 1.2$ K). Persistently large $\chi''(T)$ signals at low temperatures originate from spatially dispersed domains with disparate local T_c. Furthermore, the broad distribution of local T_c spreads the VL to VS phase transition across an extended temperature window instead of confining it to a single discrete temperature, resulting in continuous elevation of $\chi''(T)$ over a wide cooling range [41].

In $x = 0.25$ sample, under a dc field of 3 T, sharp concurrent peaks arise in both $\chi'(T)$ and $\chi''(T)$ near T_d. Such synchronized susceptibility peaks have been widely observed in various superconducting systems and are generally attributed to enhanced vortex pinning triggered by vortex lattice softening [24,26,45,46], whereas alternative studies on cuprates associate the $\chi''(T)$ peak with VS melting [44]. In our $x = 0.25$ crystal, the peak position falls within the zero-resistance regime, confirming that vortices remain trapped inside the pinned VS. Accordingly, this susceptibility peak shares identical microscopic origin with the peak effect resolved from preceding torque measurements, originating from pinning reinforcement during vortex lattice softening.

2.3. Vortex phase diagrams

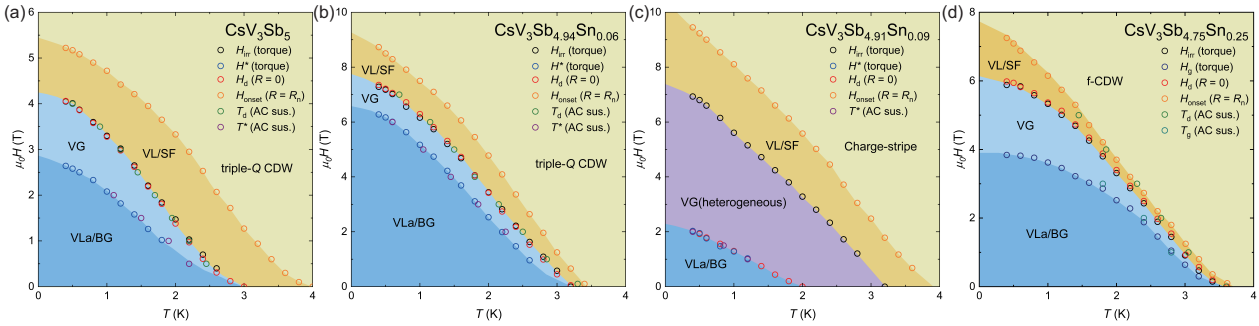


Fig. 4. The magnetic field–temperature phase diagrams of $CsV_3Sb_{5-x}Sn_x$ [$x = 0$ (a), 0.06 (b), 0.09 (c) and 0.25 (d)]. Black circles indicate the H_{irr} from magnetic torque measurements. Blue circles indicate the H^* from magnetic torque measurements in panels (a)-(c). Teal circles indicate the H_g from magnetic torque measurements in panel (d). Red circles indicate the H_d from magnetoresistance curves. Orange circles indicate the H_{onset} from magnetoresistance curves. Olive circles indicate the T_d from ac susceptibility curves. Purple circles indicate the T^* from ac susceptibility curves in panels (a)-(c). Navy circles indicate the T_g from ac susceptibility curves in panel (d). For $x = 0$, 0.06 and 0.25 samples, the phase diagram is divided into the following phases: vortex lattice (VLa)/Bragg glass (BG), vortex glass (VG), vortex liquid (VL)/superconducting fluctuations (SF) and normal state. For $x = 0.09$ sample we define a heterogeneous vortex glass state [VG(heterogeneous)].

Combining all magnetoresistance, magnetic torque and ac susceptibility data collected in the four samples, we establish the respective magnetic field–temperature phase diagrams of these superconductors. For typical type-II superconductors, in the low fields and low temperature region, the sample resides in VS phase. To distinguish two subphases of VS, the ordered VS is named vortex lattice or Bragg glass and the disordered counterpart vortex glass state (see more details in Supplemental Materials [20]). At higher magnetic fields or temperature, VS melts into VL and finally enters normal state. All characteristic

temperatures and fields of $CsV_3Sb_{5-x}Sn_x$ are summarized to construct the H–T phase diagrams of the four samples displayed in Fig. 4.

The phase diagrams for $x = 0$ and $x = 0.06$ are plotted in Fig. 4(a) and (b), respectively. H^* and T^* confirms the transition to a disordered glassy VS phase. Furthermore, $H_{\rm irr}$ nearly overlaps with $H_{\rm d}$, which strongly supports that this phase boundary separates the VS phase from either VL or superconducting fluctuation (SF) regime. The full recovery of normal state resistivity at higher temperature ($T_{\rm d}$) and magnetic field ($H_{\rm onset}$) marks the termination of superconductivity.

The phase diagram of the $x = 0.09$ sample is summarized in Fig. 4(c). Locating in the charge-stripe phase regime, this sample possesses intrinsically inhomogeneous superconductivity with spatial dispersion of local $T_{\rm c}$, which drastically differentiates its vortex phase diagram from the other three compositions. The phase transition in VS is simultaneously marked by H^*, T^* and $H_{\rm d}$. In contrast to the vortex glass states in most type-II superconductors wherein the flux lines are pinned by random disorder potential (such as point-like impurities) and are thus free from dissipative flux-flow process, the intermediate phase of $x = 0.09$ features coexisting finite non-ohmic resistivity and intact diamagnetic hysteresis. In previous studies of high-temperature superconductors, this phenomenon can arise from several mechanisms such as surface barrier [47,48] and thermally activated vortex creep [2]. In highly anisotropic superconductors Bi2212, bulk vortices remain highly mobile over a broad vortex liquid regime, whereas vortex entry and exit are still limited by thermally activated crossing of the Bean-Livingston surface barrier [47,48]. Vortex creep is the thermally activated motion of vortices between pinning sites, which causes magnetic relaxation and finite resistance [2]. At the low-current limit, dissipation caused by vortex creep is expected to be very weak. Considering the thermal fluctuations in $CsV_3Sb_{5-x}Sn_x$ should be very weak, so this behavior is unlikely dominated by conventional thermally activated vortex creep or surface barrier effects. Owing to the broad spatial $T_{\rm c}$ distribution in $x = 0.09$, magnetic irreversibility can emerge once locally connected grains form closed superconducting loops capable of trapping magnetic flux. However, these superconducting clusters do not necessarily constitute a continuous current path across the entire sample, so the macroscopic electrical resistance remains finite. Zero resistance is achieved when intergrain coupling becomes sufficiently strong to establish a sample-spanning network with long-range phase coherence. Consequently, the zero-resistance field $H_{\rm d}$ may lie below the magnetic irreversibility line $H_{\rm irr}$. We therefore define this intermediate phase as the heterogeneous vortex glass state. Upon further increasing temperature and magnetic fields, full collapse of diamagnetic hysteresis on torque curves signals a full entrance (of the entire sample) into the VL or SF regime, which are impossible to distinguish in the present case; note that this apparent $H_{\rm irr}$ is very close to the onset of normal state.

Fig. 4(d) presents the H–T phase diagram of the $x = 0.25$ sample, which is qualitatively similar to $x = 0$ and $x = 0.06$, featuring four phases. The order-disorder transition in VS is fixed by $H_{\rm g}$ and $T_{\rm g}$. The boundary separating vortex glass from VL/SF is determined by $H_{\rm d}$, $H_{\rm irr}$ and $T_{\rm d}$. The crossover from VL/SF to normal state is defined by $H_{\rm onset}$. A prominent peak effect is clearly detected in both torque and ac susceptibility of $x = 0.25$, manifesting strengthened vortex pinning across the order–disorder transition

of VS.

3. SUMMARY

Combining multiple experimental techniques including electrical transport, magnetic torque and alternating-current susceptibility measurements, we comprehensively investigate Sn-doped CsV_3Sb_5 single crystals and establish vortex phase diagrams for superconducting samples hosting distinct normal state charge orders. For $x = 0$ and $x = 0.06$ sample (SC-I), the sharp superconducting transitions in thermodynamic and transport data verify spatially homogeneous T_c across the crystal. For the $x = 0.09$ sample, magnetoresistance and torque data uncover an extensive heterogeneous vortex glass region featured by coexisting diamagnetism and finite resistance on the H–T phase diagram. Broad superconducting transitions are observed in both magnetoresistance and ac susceptibility. These features reveals intrinsic spatial T_c inhomogeneity with segregated superconducting domains in SC-II. Despite heavy Sn doping that raises residual resistivity drastically and introduces abundant native impurity pinning centers in the $x = 0.25$ sample, pronounced peak effect is clearly resolved which indicates that impurities barely trap vortices inside the ordered vortex lattice phase of SC-III; instead, effective pinning by random disorders only sets in after the system transforming into the vortex glass state.

A Systematic mapping of vortex phase diagrams across the $CsV_3Sb_{5-x}Sn_x$ unambiguously demonstrates that the form of CDW order in the normal state can impose strong influence on the superconducting properties, indicating an unconventional interplay between CDW and superconductivity in the CsV_3Sb_5 families.

Acknowledgment

Financial supports are given here. The scientific contributions from other people or groups are also acknowledged here.

We thank Zhenyu Wang for helpful discussions. This work was financially supported by the National Natural Science Foundation of China (Grants Nos. 12488201 and 12274390), theNational Key Projects for Research and Development of China (Grant No. 2022YFA1602602), the Quantum Science and Technology-National Science and Technology Major Project (Grant No. 2021ZD0302802), the Basic Research Program of the Chinese Academy of Sciences Based on MajorScientific Infrastructures (No. JZHKYPT-2021-08).

5. References

参考文献

[1] Rosenstein B and Li D 2010 *Reviews of Modern Physics* **82** 109–168

[2] Blatter G, Feigel'man M V, Geshkenbein V B, Larkin A I and Vinokur V M 1994 *Reviews of Modern Physics* **66** 1125

[3] Gurevich A 2011 *Reports on Progress in Physics* **74** 124501

[4] Hsu Y T, Berben M, Čulo M, Adachi S, Kondo T, Takeuchi T, Wang Y, Wiedmann S, Hayden S M and Hussey N E 2021 *Proceedings of the National Academy of Sciences* **118** e2016275118

[5] Yu Y and Kivelson S 2019 *Physical Review B* **99** 144513

[6] Shi Z, Baity P, Sasagawa T and Popović D 2020 *Science Advances* **6** eaay8946

[7] Ortiz B R, Teicher S M, Hu Y, Zuo J L, Sarte P M, Schueller E C, Abeykoon A M, Krogstad M J, Rosenkranz S, Osborn R *et al.* 2020 *Physical Review Letters* **125** 247002

[8] Ni S, Ma S, Zhang Y, Yuan J, Yang H, Lu Z, Wang N, Sun J, Zhao Z, Li D *et al.* 2021 *Chinese Physics Letters* **38** 057403

[9] Roppongi M, Ishihara K, Tanaka Y, Ogawa K, Okada K, Liu S, Mukasa K, Mizukami Y, Uwatoko Y, Grasset R *et al.* 2023 *Nature Communications* **14** 667

[10] Sun Y, Tu Y, Luo Y, Yu S, Li H, Zhang Y, Wu P, Wang Z, Zhang F, Ma W *et al.* 2024 *Science China Physics, Mechanics & Astronomy* **67** 277411

[11] Zhang X, Zic M P, Chen D, Shekhar C, Felser C, Fisher I R and Kapitulnik A 2024 *Physical Review B* **109** 144507

[12] Wu P, Tu Y, Wang Z, Yu S, Li H, Ma W, Liang Z, Zhang Y, Zhang X, Li Z *et al.* 2023 *Nature Physics* **19** 1143–1149

[13] Zhong Y, Liu J, Wu X, Guguchia Z, Yin J X, Mine A, Li Y, Najafzadeh S, Das D, Mielke III C *et al.* 2023 *Nature* **617** 488–492

[14] Li J, Xie W, Liu J, Li Q, Li X, Yang H, Wang Z, Yao Y and Wen H H 2022 *Physical Review B* **106** 214529

[15] Wang C, Hirota Y, Wang L, Sakagami R, Li Y, Yi X, Li W, Chen Y, Yu C, Wang Z *et al.* 2024 *Physical Review B* **109** 024514

[16] Oey Y M, Ortiz B R, Kaboudvand F, Frassineti J, Garcia E, Cong R, Sanna S, Mitrović V F, Seshadri R and Wilson S D 2022 *Physical Review Materials* **6** L041801

[17] Kautzsch L, Oey Y M, Li H, Ren Z, Ortiz B R, Pokharel G, Seshadri R, Ruff J, Kongruengkit T, Harter J W *et al.* 2023 *npj Quantum Materials* **8** 37

[18] Huai L, Wang Z, Rao H, Han Y, Liu B, Yu S, Zhang Y, Zang R, Luan R, Peng S *et al.* 2025 *Physical Review X* **15** 041039

[19] Li H *unpublished*

[20] *See Supplemental Materials for more details and explanations*

[21] Li L, Checkelsky J, Komiya S, Ando Y and Ong N 2007 *Nature Physics* **3** 311–314

[22] Xu H S, Yan Y J, Yin R, Xia W, Fang S, Chen Z, Li Y, Yang W, Guo Y and Feng D L 2021 *Physical Review Letters* **127** 187004

[23] Lyard L, Samuely P, Szabo P, Klein T, Marcenat C, Paulius L, Kim K, Jung C, Lee H S, Kang B *et al.* 2002 *Physical Review B* **66** 180502

[24] Kwok W, Fendrich J, Van der Beek C and Crabtree G 1994 *Physical Review Letters* **73** 2614

[25] Larkin A and Ovchinnikov Y N 1979 *Journal of Low Temperature Physics* **34** 409–428

[26] Giamarchi T and Le Doussal P 1997 *Physical Review B* **55** 6577

[27] Pippard A 1969 *Philosophical magazine* **19** 217–220

[28] DeSorbo W 1964 *Reviews of Modern Physics* **36** 90

[29] Berlincourt T, Hake R and Leslie D 1961 *Physical Review Letters* **6** 671

[30] Ling X and Budnick J I 1991 AC susceptibility studies of type-II superconductors: vortex dynamics *Magnetic Susceptibility of Superconductors and Other Spin Systems* (Springer) pp 377–388

[31] Higgins M J and Bhattacharya S 1996 *Physica C: Superconductivity and its applications* **257** 232–254

[32] Tinkham M 2004 *Introduction to superconductivity* (Courier Corporation)

[33] Gömöry F 1997 *Superconductor Science and Technology* **10** 523–542

[34] Bean C P 1964 *Reviews of Modern Physics* **36** 31

[35] Bean C P 1962 *Physical Review Letters* **8** 250

[36] Francavilla T L, Hein R A and Liebenberg D H 2013 *Magnetic susceptibility of superconductors and other spin systems* (Springer Science & Business Media)

[37] Kes P, Aarts J, Van den Berg J, Van der Beek C and Mydosh J 1989 *Superconductor Science and Technology* **1** 242–248

[38] Geshkenbein V, Vinokur V and Fehrenbacher R 1991 *Physical Review B* **43** 3748

[39] Anderson P W and Kim Y 1964 *Reviews of Modern Physics* **36** 39

[40] Nikolo M and Goldfarb R B 1989 *Physical Review B* **39** 6615

[41] Muller K H, Collocott S, Driver R and Savvides N 1991 *Superconductor Science and Technology* **4** S325–S327

[42] Prando G, Carretta P, De Renzi R, Sanna S, Palenzona A, Putti M and Tropeano M 2011 *Physical Review B* **83** 174514

[43] Ishida T, Okuda K, Rykov A I, Tajima S and Terasaki I 1998 *Physical Review B* **58** 5222

[44] Ishida T, Okuda K and Asaoka H 1997 *Physical Review B* **56** 5128

[45] Ge J, Gutierrez J, Li J, Yuan J, Wang H B, Yamaura K, Takayama-Muromachi E and Moshchalkov V 2013 *Physical Review B* **88** 144505

[46] Pasquini G, Daroca D P, Chiliotte C, Lozano G and Bekeris V 2008 *Physical Review Letters* **100** 247003

[47] Chikumoto N, Konczykowski M, Motohira N and Malozemoff A 1992 *Physical Review Letters* **69** 1260

[48] Fuchs D T, Zeldov E, Rappaport M, Tamegai T, Ooi S and Shtrikman H 1998 *Nature* **391** 373–376